NANO LETTERS

pubs.acs.org/NanoLett Letter

In Situ Prelithiation by Direct Integration of Lithium Mesh into Battery Cells

Yufei Yang, Jiangyan Wang, Sang Cheol Kim, Wenbo Zhang, Yucan Peng, Pu Zhang, Rafael A. Vilá, Yinxing Ma, You Kyeong Jeong, and Yi Cui*

Cite This: *Nano Lett.* 2023, 23, 5042–5047 Read Online

ACCESS | Metrics & More | Article Recommendations | Supporting Information

ABSTRACT: Silicon (Si)-based anodes are promising for next-generation lithium (Li)-ion batteries due to their high theoretical capacity (∼3600 mAh/g). However, they suffer quantities of capacity loss in the first cycle from initial solid electrolyte interphase (SEI) formation. Here, we present an *in situ* prelithiation method to directly integrate a Li metal mesh into the cell assembly. A series of Li meshes are designed as prelithiation reagents, which are applied to the Si anode in battery fabrication and spontaneously prelithiate Si with electrolyte addition. Various porosities of Li meshes tune prelithiation amounts to control the degree of prelithiation precisely. Besides, the patterned mesh design enhances the uniformity of prelithiation. With an optimized prelithiation amount, the *in situ* prelithiated Si-based full cell shows a constant >30% capacity improvement in 150 cycles. This work presents a facile prelithiation approach to improve battery performance.

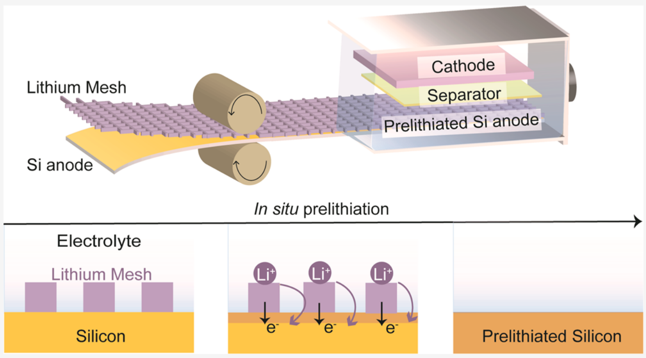

KEYWORDS: *lithium-ion battery, prelithiation, silicon anode*

Initial Coulombic efficiency (CE) is a critical index for lithium-ion battery (LIBs) performance as it is directly related to the battery capacity in later cycling. In a conventional LIB, the solid-electrolyte interphase (SEI) formed in the initial cycle irreversibly consumes some active Li ions, causing the incomplete utilization of active materials and compromised battery capacity.[1−4] This problem is particularly severe in silicon (Si)-based LIBs. Silicon anodes have high theoretical capacity (3579 mAh/g), 10 times higher than that of conventional graphite anodes (372 mAh/g), and hold great potential for application in high-energy LIBs.[5,6] However, Si experiences significant SEI formation in the initial cycle due to the high surface area of nanosized silicon and electrochemical instability with the electrolyte. Thus, Si exhibits a low initial CE of 50−80%,[7−9] indicating a loss of 20−50% battery capacity after the initial cycle. Therefore, a strategy to compensate for the initial active Li^+ loss and improve the initial CE is needed to prevent battery energy density degradation.

Prelithiation, a strategy to pre-emptively lithiate the electrodes for active Li^+ loss compensation, has attracted considerable attention. Several distinct methods of prelithiation have been proposed. An ideal prelithiation strategy requires high efficiency, high compatibility with the existing battery fabrication process, and precise control. However, current prelithiation methods seldom fulfill all requirements. Stabilized lithium metal powder (SLMP)[10−12] and a series of lithium alloying particles[9,13−15] were developed as prelithiation additives for the electrode slurry. While the prelithiation amount can be precisely adjusted by the additive amount, their compatibility issues with the conventional solvents used in electrode slurry preparation limit their applications. Electrochemical prelithiation[16−18] also provides precise control, but the required cell disassembly and reassembly lead to low compatibility with the current battery manufacturing process. Recently, a chemical prelithiation approach has been developed via immersing electrodes in highly reductive solutions, such as Li-Naph[19] and Li-Bp.[20,21] However, the high reactivity of these solutions poses safety concerns for large-scale battery manufacturing. Additionally, adjusting the prelithiation degree by varying the reaction time may reduce the controllability of the process. Direct contact with lithium is another prelithiation strategy that is fast and facile. However, excess lithium is often used in previous studies that require residual Li removal after prelithiation,[22,23] which increases the

Received: March 9, 2023
Revised: May 22, 2023
Published: May 26, 2023

https://doi.org/10.1021/acs.nanolett.3c00859
Nano Lett. 2023, 23, 5042−5047

difficulty in both manufacturing and control of the prelithiation amount. Thermal evaporation can precisely control the Li thickness,[24] but the approach has a high technical barrier. Therefore, prelithiation techniques demand further improvement and understanding for practical applications.

Here, we present an *in situ* prelithiation method with high efficiency, high compatibility, and precise control. This prelithiation process takes one step to apply the Li mesh to the Si anode during battery fabrication, which eliminates the need for cell disassembly and reduces electrolyte waste. Upon adding electrolyte to the battery, prelithiation happens spontaneously between contacted Si and Li based on the shorting mechanism. The prelithiation capacity is tuned by the Li mesh porosity to precisely control the prelithiation degree. By utilizing *in situ* prelithiation with optimized Li mesh porosity, the initial CE of the Si-based half-cell is improved from ~70 to ~100%. In addition, the patterned design of the Li mesh facilitates Li diffusion for more uniform prelithiation. Scanning electron microscopy (SEM) and X-ray photoelectron spectroscopy (XPS) reveal both morphological and chemical uniformity in different regions of the prelithiated Si electrodes. Furthermore, the prelithiated Si-based full cell shows long-cycle capacity improvement by over 30% in 150 cycles. Therefore, *in situ* prelithiation via Li mesh demonstrates a promising prelithiation design for practical applications.

The *in situ* prelithiation approach involves applying a layer of Li mesh to the Si anode during battery assembly (Figure 1a).

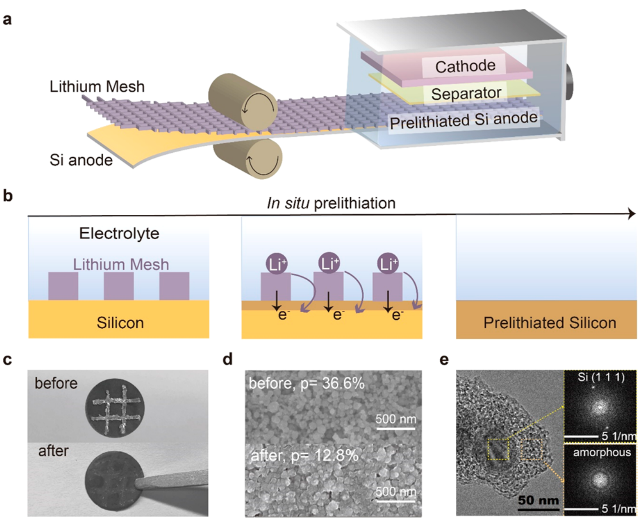

Figure 1. Design of *in situ* prelithiation. (a) Schematic of *in situ* prelithiation process by applying a layer of the Li mesh to the silicon anode during battery fabrication. (b) Mechanism of the *in situ* prelithiation reaction based on shorting. (c) Digital photographs of the Si anode before (upper) and after (bottom) 24 h *in situ* prelithiation by Li mesh. (d) SEM images of the Si anode before (upper) and after (bottom) 24 h *in situ* prelithiation by Li mesh. (e) TEM and selected-area FFT images (calculated from HRTEM images collected in the highlighted regions, Supporting Information Figure S3d) of a Si particle after 24 h of prelithiation.

After assembly, the Li mesh in direct contact with the Si anode is surrounded by the electrolyte, which leads to shorting between the Si anode and the Li mesh. The chemical reaction of prelithiation is shown below:

$$\text{Li mesh: } x\text{Li} \rightarrow x\text{Li}^{+} + xe^{-}$$

$$\text{Si: Si} + x\text{Li}^{+} + xe^{-} \rightarrow \text{Li}_x\text{Si}$$

$$\text{net reaction: } x\text{Li} + \text{Si} \rightarrow \text{Li}_x\text{Si}$$

As illustrated in Figure 1b, electrons can be transported from the Li mesh directly to the Si anode by the Si−Li contact points, while Li^+ can diffuse from Li to Si through the electrolyte. The reaction has a Gibbs free energy of −36 kJ/mol, indicating that this reaction is thermodynamically spontaneous. Thus, our prelithiation approach happens in the battery resting period after electrolyte injection. As shown in Figure 1c, inserted Li mesh is fully consumed after *in situ* prelithiation, illustrating that prelithiation is complete after a 24 h simultaneous resting and prelithiation period. This result is also supported by X-ray diffraction (XRD) spectra (Supporting Information Figure S1), where no crystalline peaks of Li were detected. Scanning electron microscopy (SEM) and transmission electron microscopy (TEM) characterizations display Si particles expanding and fusing after 24 h of resting, with the electrode thickness increasing from 12 to 27 μm (Supporting Information Figure S2) and the porosity of the Si electrode decreasing from 36.6 to 12.8% (Figure 1d, Supporting Information Figure S3a,b). These phenomena indicate Si−Li alloying and demonstrate successful prelithiation.[25,26] Moreover, we observe a core−shell structure of prelithiated Si particles (Figure 1e). The Si nanoparticle before prelithiation is crystalline with a thin SiO_2 amorphous layer (<2 nm) (Supporting Information Figure S3c). In the prelithiated Si particle, the inner core remains crystalline but the outer shell becomes amorphous Li_xSi,[27,28] which is a typical lithiation behavior for Si during the first cycle.[29]

In addition to its simplicity, our *in situ* prelithiation approach offers a precision advantage. When porous patterns are introduced into Li foils, the Li mesh capacity is reduced to match the initial capacity loss of the Si anode, enabling precise prelithiation. A series of Li meshes with varied porosity of 50% (p-50), 60% (p-60), 70% (p-70), and 80% (p-80) were designed and fabricated (Figure 2a, Supporting Information Note 1), with storage capacities of around 2.5, 2, 1.5, and 1 mAh/cm^2, respectively, based on the 25-μm-thick lithium foil used in this project (Figure 2b, Supporting Information Note 2). To verify the precision of our prelithiation approach, Si||Li metal half-cells were fabricated to evaluate the initial CE improvement. Figure 2c summarizes the initial CE values of Si samples under different prelithiation conditions. For the pristine Si anode, the initial CE is ~70%. Based on the initial CE and the mass loading of the Si anode (1.4 ± 0.15 mg/cm^2), the initial capacity loss/desired prelithiation capacity is estimated to be ~1.5 mAh/cm^2 through calculation (Supporting Information Note 3). The p-80 Li mesh, with an insufficient capacity of 1 mAh/cm^2, only partially compensated for the initial capacity loss and improved the initial CE to ~95%. Meanwhile, p-70 Li mesh with the desired capacity of 1.5 mAh/cm^2 successfully improves the CE to ~100%. The p-60 and p-50 Li meshes, with excess capacities of 2 and 2.5 mAh/cm^2, overprelithiated the Si anodes and improved the initial CE far above 100% (Supporting Information Figure S4). The precision of our prelithiation approach is further illustrated in Figure 2d. In this pristine Si sample, the irreversible Li loss in the first cycle is ~1.35 mAh/cm^2, as indicated by the capacity difference between the first cycle charge and discharge profile. After prelithiation with a p-80 (1 mAh/cm^2) Li mesh, the initial CE of the Si anode is improved

https://doi.org/10.1021/acs.nanolett.3c00859
Nano Lett. 2023, 23, 5042−5047

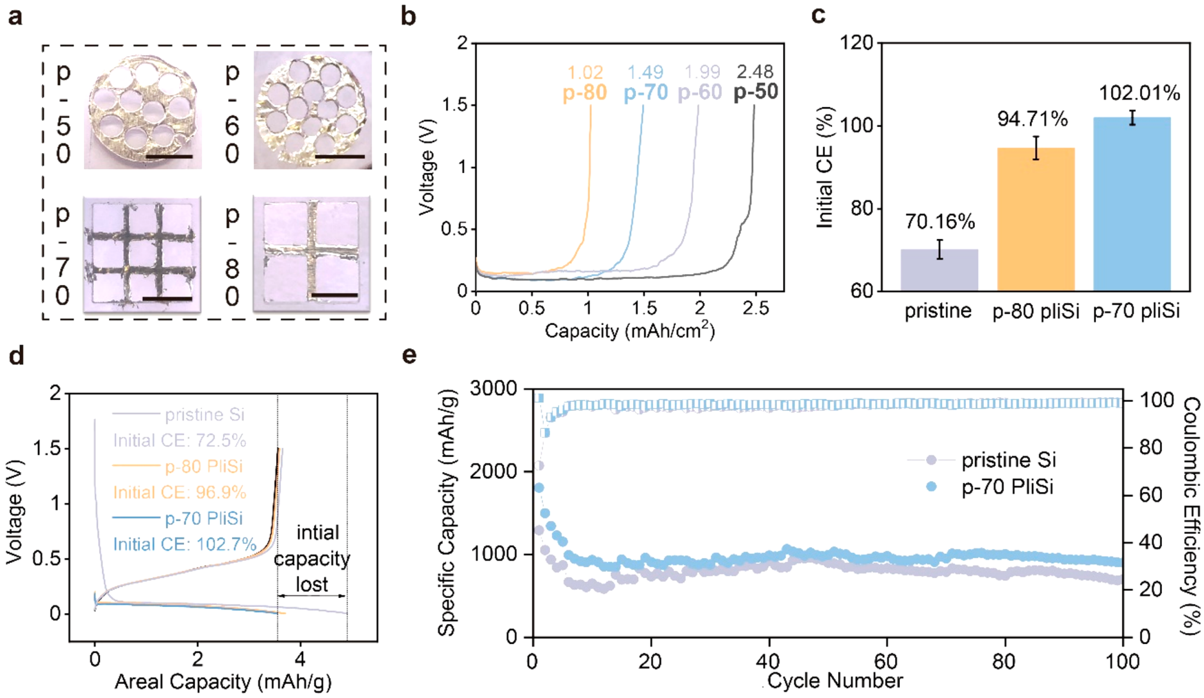

Figure 2. Precise control of prelithiation degree. (a) Digital photographs of Li meshes with different porosities varied from 50 to 80%; the scale bar is 5 mm. (b) Voltage−capacity profiles of Li meshes, showing the stored Li capacity in these meshes. (c) Initial CE of multiple silicon samples using different porosities of Li meshes for prelithiation. Four parallel samples were recorded for each prelithiation condition. (d) First-cycle voltage profiles of the pristine Si and p-70 and p-80 Li mesh prelithiated Si, respectively. The gap between two dashed lines indicates the capacity loss in the first cycle. (e) Cycling performance of pristine Si anode and Si prelithiated by p-70 Li mesh (current @ 180 mA/g).

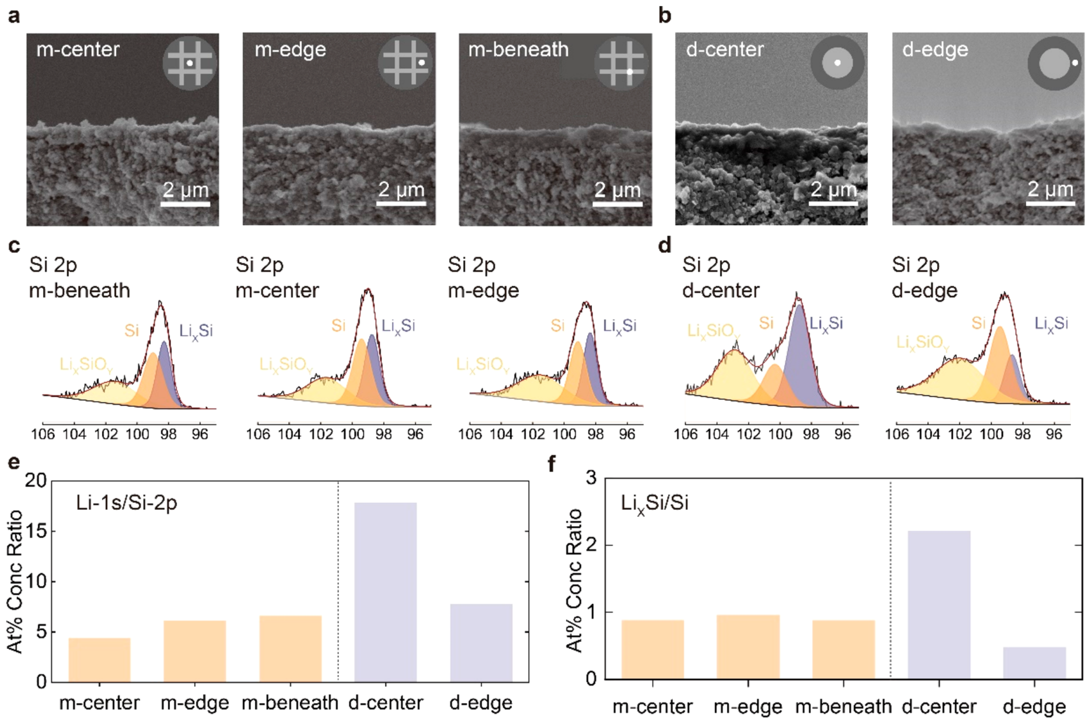

Figure 3. Morphological and chemical uniformity. (a) Cross-sectional SEM images of the Li-mesh prelithiated Si anode at three locations, center (m-center), edge (m-edge), and beneath (m-beneath), shown in the inset schematics. (b) Cross-sectional SEM images of the Li-disk prelithiated Si anode of two different zones, center (d-center) and edge (d-edge). (c) Si 2p XPS spectra of the Li-mesh prelithiated Si anode of three different zones; the sputtering time is 0.5 min. (d) Si 2p XPS spectra of the Li-disk prelithiated Si anode of two different zones; the sputtering time is 0.5 min. (e) Li 1s and Si 2p atomic concentration ratio in Li-mesh prelithiation and Li-disk prelithiation. (f) Li_xSi and Si atomic concentration ratio in Li-mesh prelithiation and Li-disk prelithiation.

https://doi.org/10.1021/acs.nanolett.3c00859
Nano Lett. 2023, 23, 5042−5047

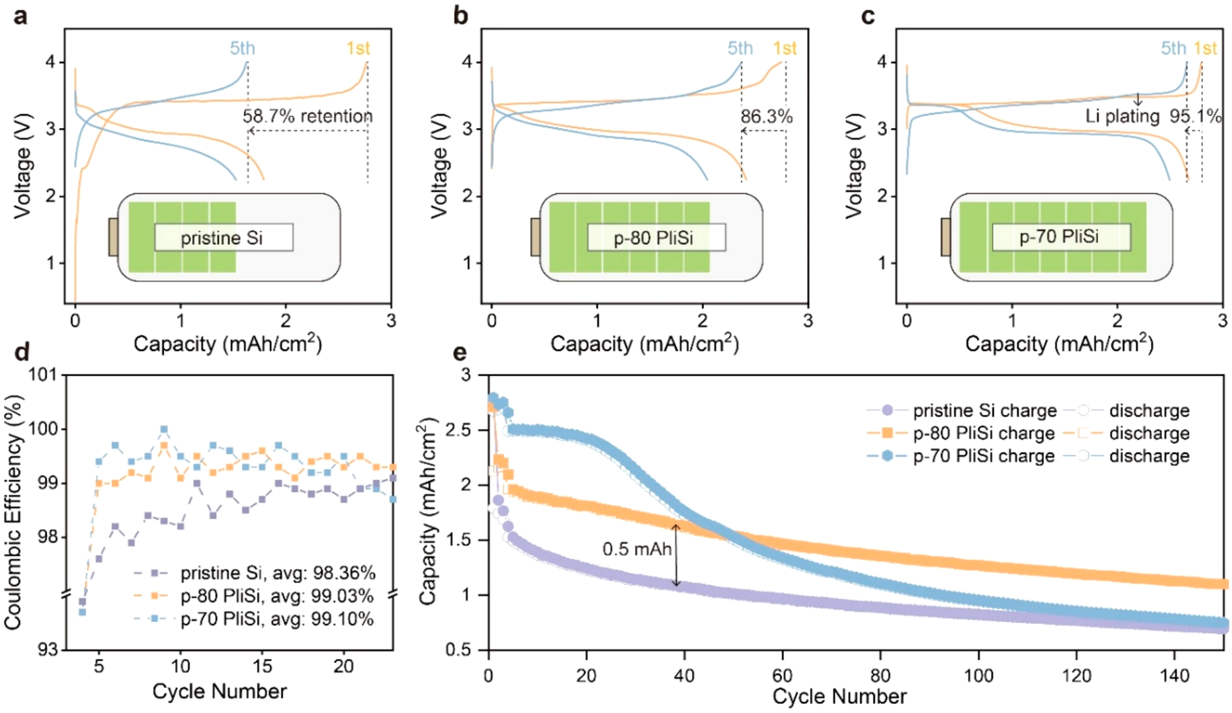

Figure 4. Capacity improvement in prelithiated full batteries. (a−c) Voltage profiles of Si-LFP batteries of the first cycle (0.05 C, preactivation cycle) and the fifth cycle (0.25 C) with embedded schematics showing the capacity retention: pristine Si (a), prelithiated Si by p-80 Li mesh (b), and prelithiated Si by p-70 Li mesh (c). (d) Coulombic efficiency of the first 20 cycles of Si-LFP full cells using pristine Si, p-80 Li mesh prelithiated Si, and p-70 Li mesh prelithiated Si, respectively (the first three activation cycles are not included). (e) Full-cell cycling performance of pristine Si, p-80 Li mesh prelithiated Si, and p-70 Li mesh prelithiated Si, respectively.

from 72.5 to 96.9%. In contrast, prelithiation with a p-70 (1.5 mAh/cm^2) Li mesh, whose capacity is slightly above the desired prelithiation capacity, improves the initial CE to 102.7%. These results demonstrate the precise control in the Li-mesh prelithiation method. It can achieve ∼100% initial CE by matching the Li mesh capacity with the initial capacity loss. Additionally, it is worth noting that pristine and prelithiated Si anodes present similar delithiation curves, indicating that our prelithiation approach does not alter the electrochemical behavior of the Si anode. The slightly more stable cycling behavior of the prelithiated Si anode compared to pristine Si (Figure 2e) further confirms that our *in situ* prelithiation method does not deteriorate the cycling performance of the Si anode.

Aside from simplicity and precision, our prelithiation method achieves reasonable uniformity through Li mesh patterning. Uneven prelithiation is not ideal because the accompanying irregular volume expansion is likely to cause high local stress and thus produce suboptimal electrode performance.[30] To investigate the uniformity of our prelithiation method, a patterned p-70 Li mesh was used as an example prelithiation reagent whose grid structure divided the Si anode into nine zones, among which one center (m-center), one edge (m-edge), and one zone beneath the Li mesh (m-beneath) were chosen for SEM and XPS characterizations (Supporting Information Figure S5a). In comparison, a centralized Li disk with the same effective mass was fabricated where one center (d-center) and one edge (d-edge) zone were chosen for study (Supporting Information Figure S5b). As shown in Figure 3a, the cross-sectional SEM images of the Li-mesh prelithiated Si anode in three different zones show similar features. On the contrary, in Li-disk prelithiation (Figure 3b), the central zone shows a higher degree of prelithiation than the edge zone at the electrode surfaces, indicating less uniformity without Li-mesh design. Besides morphological homogeneity, further XPS study demonstrates the chemical uniformity of the prelithiated Si anode using a Li-mesh design. High-resolution spectra of Si 2p and Li 1s peaks in three zones of Li-mesh prelithiation and two zones of Li-disk prelithiation were acquired (Figure 3c,d, Supporting Information Figure S6). The Si 2p peak was deconvoluted into three components: Li_xSi at 98.2 eV, Si at 99.2 eV, and Li_xSiO_y at ∼102 eV.[31,32] As shown in Figure 3c, the Li-mesh prelithiated Si anode displays similar chemical compositions in the three studied zones, indicating prelithiation homogeneity. However, in the Li-disk prelithiation (Figure 3d), the central area shows less Si but more Li_xSi than the edge area, indicating a higher prelithiation degree in the central area. This heterogeneity likely results from the difficulty of Li^+ diffusion from the Li dish to the edge. Figure 3e,f summarizes the atomic concentration ratios of Li-1s/Si-2p and Li_xSi/Si, respectively. In contrast to the significant discrepancy observed in centralized Li-disk prelithiation, the patterned Li mesh offers a clear advantage in homogeneity. Besides horizontal uniformity, the vertical uniformity is also investigated via cross-sectional SEM-EDX (Supporting Information Figure S7), showing the uniform distribution of Si, C, O, and F elements across the electrode thickness. The demonstrated morphological and chemical homogeneity in Li-mesh prelithiation reveals the necessity of a Li-mesh design.

We further demonstrate that our *in situ* prelithiation can effectively improve the full-cell cycling capacity. In a full battery, limited Li sources are originally stored in the cathode. When part of the active Li is consumed in SEI formation in the

https://doi.org/10.1021/acs.nanolett.3c00859
Nano Lett. 2023, 23, 5042−5047

first cycle, this active Li loss irreversibly diminishes the retained capacity. Prelithiation, however, by adding sacrificial Li sources for compensation, improves capacity retention in batteries for later cycling. Here, we paired Si anodes with lithium iron phosphate (LFP) cathodes to construct full cells for demonstration. Graphene-coated porous Si (g@pSi) was used here for better mechanical stability.[33,34] The first three cycles were conducted at 0.05 C (0.14 mA/cm^2) for activation before later cycles at 0.25 C (0.7 mA/cm^2). In Figure 4a−c, we compare the voltage profiles of the first cycle and the fifth cycle of pristine Si, p-80 Li mesh prelithiated Si (p-80 PliSi), and p-70 Li mesh prelithiated Si (p-70 PliSi), respectively. The charge capacity of the first activation cycle represents the designed battery capacity, and the charge capacity of the fifth cycle represents the practical capacity of the battery at a normal cycling rate. Pristine Si exhibits only 58.7% retention of the designed capacity, with about 1 mAh/cm^2 capacity loss (Figure 4a). Prelithiation with p-80 Li mesh (~1 mAh/cm^2) compensates well for the initial capacity loss, which increases the capacity retention by ~1/3 of the designed capacity to 86.3% (Figure 4b). We further evaluate the overprelithiation condition with p-70 Li mesh prelithiation (~1.5 mAh/cm^2). Although the capacity retention is improved to 95.1%, comparable to that of the Li-LFP half-cell (97.1%), the voltage plateau at 3.5 V in charging indicates Li metal plating (Figure 4c, Supporting Information Figure S8). It is noteworthy that prelithiation improves the CE via a lasting effect, not only in the first cycle. As shown in Figure 4d, the average CE of the first 20 cycles (excluding the first three activation cycles) is increased from 98.36 to over 99% with prelithiation. This improvement is possible from the well-preformed SEI in the prelithiated Si (Supporting Information Figure S9); meanwhile, the SEI in pristine Si takes longer cycles to fully establish. Moreover, the prominence of prelithiation in improving the battery practical capacity is evidently revealed in Figure 4e. The nonprelithiated battery and prelithiated battery exhibit similar initial charge capacities, indicating a similar battery design capacity. Prelithiation with the matched prelithiation amount by p-80 Li mesh provides a constant 0.5 mAh/cm^2 higher capacity than that of pristine Si for 150 cycles, corresponding to more than a 30% capacity increase. Overprelithiation with p-70 Li mesh remains high capacity in the initial 20 cycles but experiences quick capacity decay afterward, possibly due to the deterioration from Li metal plating. This result reveals the importance of preventing an excessive sacrificial amount of Li in prelithiation.

In this work, we developed an *in situ* prelithiation approach to effectively compensate for the battery irreversible initial capacity loss. Our approach involves applying a layer of Li mesh to the Si anode in battery fabrication, which enables spontaneous prelithiation via shorting during the battery resting period. By tuning the porosity of the Li mesh, we can precisely control the prelithiation capacity. Matching the Li mesh capacity with the initial capacity loss enables us to significantly improve the initial CE of Si anodes, from around 70 to 100%. The prelithiation of Si anodes in full cells also results in a >30% improvement in long-term battery capacity over 150 cycles. Furthermore, the Li mesh design facilitates Li diffusion for uniform prelithiation. This work provides new insights for the development of prelithiation strategies for high-energy-density Si anodes.

ASSOCIATED CONTENT

Supporting Information

The Supporting Information is available free of charge at https://pubs.acs.org/doi/10.1021/acs.nanolett.3c00859.

Experimental details, characterization methods, and supplementary figures and notes (PDF)

AUTHOR INFORMATION

Corresponding Author

Yi Cui − *Department of Materials Science and Engineering, Stanford University, Stanford, California 94305, United States; Stanford Institute for Materials and Energy Sciences, SLAC National Accelerator Laboratory, Menlo Park, California 94025, United States*; orcid.org/0000-0002-6103-6352; Email: yicui@stanford.edu

Authors

Yufei Yang − *Department of Materials Science and Engineering, Stanford University, Stanford, California 94305, United States*; orcid.org/0000-0002-3480-095X

Jiangyan Wang − *Department of Materials Science and Engineering, Stanford University, Stanford, California 94305, United States*

Sang Cheol Kim − *Department of Materials Science and Engineering, Stanford University, Stanford, California 94305, United States*; orcid.org/0000-0002-1749-8277

Wenbo Zhang − *Department of Materials Science and Engineering, Stanford University, Stanford, California 94305, United States*

Yucan Peng − *Department of Materials Science and Engineering, Stanford University, Stanford, California 94305, United States*

Pu Zhang − *Department of Materials Science and Engineering, Stanford University, Stanford, California 94305, United States*

Rafael A. Vilá − *Department of Materials Science and Engineering, Stanford University, Stanford, California 94305, United States*

Yinxing Ma − *Department of Materials Science and Engineering, Stanford University, Stanford, California 94305, United States*

You Kyeong Jeong − *Department of Materials Science and Engineering, Stanford University, Stanford, California 94305, United States*

Complete contact information is available at: https://pubs.acs.org/10.1021/acs.nanolett.3c00859

Author Contributions

Y.C. and Y.Y. conceived the idea for the project. Y.Y. and J.W. designed the experiments. Y.Y., S.C.K., and Y.K.J. fabricated the electrodes. Y.P. conducted the laser cutting for the Li mesh mode. Y.Y. fabricated the Li mesh, conducted the SEM characterizations, and designed and conducted the electrochemical measurements. R.A.V. conducted the TEM characterizations. Y.M. conducted the XRD characterizations. All authors contributed to the data discussions. Y.Y. and Y.C. wrote and revised the manuscript with input from all authors.

Notes

The authors declare no competing financial interest.

■ ACKNOWLEDGMENTS

This work was supported by the Assistant Secretary for Energy Efficiency and Renewable Energy, Office of Vehicle Technologies of the U.S. Department of Energy under the Battery Materials Research program. Part of this work was performed at the Stanford Nano Shared Facilities (SNSF), supported by the National Science Foundation under award ECCS-1542152. Y.C. acknowledges the commercialized 25-μm-thick pure Li metal foil provided by the Hydro-Québec Company.

■ REFERENCES

(1) Li, X.; Sun, X.; Hu, X.; Fan, F.; Cai, S.; Zheng, C.; Stucky, G. D. Review on comprehending and enhancing the initial Coulombic efficiency of anode materials in lithium-ion/sodium-ion batteries. *Nano Energy* **2020**, *77*, 105143.

(2) Sun, C.; Zhang, X.; Li, C.; Wang, K.; Sun, X.; Ma, Y. Recent advances in prelithiation materials and approaches for lithium-ion batteries and capacitors. *Energy Storage Mater.* **2020**, *32*, 497.

(3) Sun, Y.; Lee, H.-W.; Seh, Z. W.; Liu, N.; Sun, J.; Li, Y.; Cui, Y. High-capacity battery cathode prelithiation to offset initial lithium loss. *Nat. Energy* **2016**, *1*, 15008.

(4) Zhan, R.; Wang, X.; Chen, Z.; Seh, Z. W.; Wang, L.; Sun, Y. Promises and challenges of the practical implementation of prelithiation in lithium-ion batteries. *Adv. Energy Mater.* **2021**, *11* (35), 2101565.

(5) Chan, C. K.; Peng, H.; Liu, G.; McIlwrath, K.; Zhang, X. F.; Huggins, R. A.; Cui, Y. High-performance lithium battery anodes using silicon nanowires. *Nat. Nanotechnol.* **2008**, *3* (1), 31−35.

(6) Liu, Y.; Zhou, G.; Liu, K.; Cui, Y. Design of complex nanomaterials for energy storage: past success and future opportunity. *Acc. Chem. Res.* **2017**, *50* (12), 2895−2905.

(7) Zuo, X.; Zhu, J.; Müller-Buschbaum, P.; Cheng, Y.-J. Silicon based lithium-ion battery anodes: A chronicle perspective review. *Nano Energy* **2017**, *31*, 113−143.

(8) Zhu, B.; Wang, X.; Yao, P.; Li, J.; Zhu, J. Towards high energy density lithium battery anodes: silicon and lithium. *Chem. Sci.* **2019**, *10* (30), 7132−7148.

(9) Zhao, J.; Lu, Z.; Liu, N.; Lee, H.-W.; McDowell, M. T.; Cui, Y. Dry-air-stable lithium silicide−lithium oxide core−shell nanoparticles as high-capacity prelithiation reagents. *Nat. Commun.* **2014**, *5*, 5088.

(10) Forney, M. W.; Ganter, M. J.; Staub, J. W.; Ridgley, R. D.; Landi, B. J. Prelithiation of silicon−carbon nanotube anodes for lithium ion batteries by stabilized lithium metal powder (SLMP). *Nano Lett.* **2013**, *13* (9), 4158−4163.

(11) Jarvis, C.; Lain, M.; Yakovleva, M.; Gao, Y. A prelithiated carbon anode for lithium-ion battery applications. *J. Power Sources* **2006**, *162* (2), 800−802.

(12) Pu, K.; Qu, X.; Zhang, X.; Hu, J.; Gu, C.; Wu, Y.; Gao, M.; Pan, H.; Liu, Y. Nanoscaled lithium powders with protection of ionic liquid for highly stable rechargeable lithium metal batteries. *Adv. Sci.* **2019**, *6* (24), 1901776.

(13) Li, X.; Kersey-Bronec, F. E.; Ke, J.; Cloud, J. E.; Wang, Y.; Ngo, C.; Pylypenko, S.; Yang, Y. Study of lithium silicide nanoparticles as anode materials for advanced lithium ion batteries. *ACS Appl. Mater. Interfaces* **2017**, *9* (19), 16071−16080.

(14) Zhao, J.; Lu, Z.; Wang, H.; Liu, W.; Lee, H.-W.; Yan, K.; Zhuo, D.; Lin, D.; Liu, N.; Cui, Y. Artificial solid electrolyte interphase-protected Li x Si nanoparticles: An efficient and stable prelithiation reagent for lithium-ion batteries. *J. Am. Chem. Soc.* **2015**, *137* (26), 8372−8375.

(15) Zhao, J.; Sun, J.; Pei, A.; Zhou, G.; Yan, K.; Liu, Y.; Lin, D.; Cui, Y. A general prelithiation approach for group IV elements and corresponding oxides. *Energy Storage Mater.* **2018**, *10*, 275−281.

(16) Kim, H. J.; Choi, S.; Lee, S. J.; Seo, M. W.; Lee, J. G.; Deniz, E.; Lee, Y. J.; Kim, E. K.; Choi, J. W. Controlled prelithiation of silicon monoxide for high performance lithium-ion rechargeable full cells. *Nano Lett.* **2016**, *16* (1), 282−288.

(17) Zhou, H.; Wang, X.; Chen, D. Li-Metal-Free Prelithiation of Si-Based Negative Electrodes for Full Li-Ion Batteries. *ChemSusChem* **2015**, *8* (16), 2737−2744.

(18) Rezqita, A.; Kathribail, A.-R.; Kahr, J.; Jahn, M. Analysis of Degradation of Si/Carbon‖ LiNi0. 5Mn0. 3Co0. 2O2 Full Cells: Effect of Prelithiation. *J. Electrochem. Soc.* **2019**, *166* (3), A5483.

(19) Shen, Y.; Qian, J.; Yang, H.; Zhong, F.; Ai, X. Chemically Prelithiated Hard-Carbon Anode for High Power and High Capacity Li-Ion Batteries. *Small* **2020**, *16* (7), 1907602.

(20) Wang, G.; Li, F.; Liu, D.; Zheng, D.; Luo, Y.; Qu, D.; Ding, T.; Qu, D. Chemical prelithiation of negative electrodes in ambient air for advanced lithium-ion batteries. *ACS Appl. Mater. Interfaces* **2019**, *11* (9), 8699−8703.

(21) Yan, M.-Y.; Li, G.; Zhang, J.; Tian, Y.-F.; Yin, Y.-X.; Zhang, C.-J.; Jiang, K.-C.; Xu, Q.; Li, H.-L.; Guo, Y.-G. Enabling SiO x/C anode with high initial coulombic efficiency through a chemical pre-lithiation strategy for high-energy-density lithium-ion batteries. *ACS Appl. Mater. Interfaces* **2020**, *12* (24), 27202−27209.

(22) Liu, N.; Hu, L.; McDowell, M. T.; Jackson, A.; Cui, Y. Prelithiated silicon nanowires as an anode for lithium ion batteries. *ACS Nano* **2011**, *5* (8), 6487−6493.

(23) Shellikeri, A.; Watson, V.; Adams, D.; Kalu, E.; Read, J.; Jow, T.; Zheng, J.; Zheng, J. Investigation of pre-lithiation in graphite and hard-carbon anodes using different lithium source structures. *J. Electrochem. Soc.* **2017**, *164* (14), A3914.

(24) Kim, K.; Shon, J.; Jeong, H.; Park, H.; Lim, S.-J.; Heo, J. Improving the cyclability of silicon anodes for lithium-ion batteries using a simple pre-lithiation method. *J. Power Sources* **2020**, *459*, 228066.

(25) Jang, J.; Kang, I.; Choi, J.; Jeong, H.; Yi, K.-W.; Hong, J.; Lee, M. Molecularly tailored lithium−arene complex enables chemical prelithiation of high-capacity lithium-ion battery anodes. *Angew. Chem., Int. Ed.* **2020**, *59* (34), 14473−14480.

(26) Luo, L.; Wu, J.; Luo, J.; Huang, J.; Dravid, V. P. Dynamics of electrochemical lithiation/delithiation of graphene-encapsulated silicon nanoparticles studied by in-situ TEM. *Sci. Rep.* **2014**, *4*, 3863.

(27) Huang, W.; Wang, J.; Braun, M. R.; Zhang, Z.; Li, Y.; Boyle, D. T.; McIntyre, P. C.; Cui, Y. Dynamic structure and chemistry of the silicon solid-electrolyte interphase visualized by cryogenic electron microscopy. *Matter* **2019**, *1* (5), 1232−1245.

(28) Wang, J.; Liao, L.; Lee, H. R.; Shi, F.; Huang, W.; Zhao, J.; Pei, A.; Tang, J.; Zheng, X.; Chen, W. Surface-engineered mesoporous silicon microparticles as high-Coulombic-efficiency anodes for lithium-ion batteries. *Nano Energy* **2019**, *61*, 404−410.

(29) Ding, N.; Xu, J.; Yao, Y.; Wegner, G.; Fang, X.; Chen, C.; Lieberwirth, I. Determination of the diffusion coefficient of lithium ions in nano-Si. *Solid State Ion.* **2009**, *180* (2−3), 222−225.

(30) Yang, K.; Zhang, Y.; Wang, F.; Tang, M. Understand and Mitigate Reaction Non-Uniformity in Battery Electrodes. *ECS Meet. Abstr.* **2019**, *MA2019-01*, 94.

(31) Cao, C.; Abate, I. I.; Sivonxay, E.; Shyam, B.; Jia, C.; Moritz, B.; Devereaux, T. P.; Persson, K. A.; Steinruck, H.-G.; Toney, M. F. Solid electrolyte interphase on native oxide-terminated silicon anodes for Li-ion batteries. *Joule* **2019**, *3* (3), 762−781.

(32) Chen, J.; Fan, X.; Li, Q.; Yang, H.; Khoshi, M. R.; Xu, Y.; Hwang, S.; Chen, L.; Ji, X.; Yang, C. Electrolyte design for LiF-rich solid−electrolyte interfaces to enable high-performance microsized alloy anodes for batteries. *Nat. Energy* **2020**, *5* (5), 386−397.

(33) Wang, J.; Huang, W.; Kim, Y. S.; Jeong, Y. K.; Kim, S. C.; Heo, J.; Lee, H. K.; Liu, B.; Nah, J.; Cui, Y. Scalable synthesis of nanoporous silicon microparticles for highly cyclable lithium-ion batteries. *Nano Res.* **2020**, *13*, 1558.

(34) Kim, S. C.; Huang, W.; Zhang, Z.; Wang, J.; Kim, Y.; Jeong, Y. K.; Oyakhire, S. T.; Yang, Y.; Cui, Y. Graphene coating on silicon anodes enabled by thermal surface modification for high-energy lithium-ion batteries. *MRS Bull.* **2022**, *47* (2), 127−133.

https://doi.org/10.1021/acs.nanolett.3c00859
Nano Lett. 2023, 23, 5042−5047